Available online at www.sciencedirect.com
ScienceDirect
Journal of Hazardous Materials 148 (2007) 679–692
Journal of Hazardous Materials
www.elsevier.com/locate/jhazmat

Characterization of dissolved organic matter in leachate discharged from final disposal sites which contained municipal solid waste incineration residues

Dong-June Seo [a], Yong-Jin Kim [b,*], Sang-Yee Ham [a], Dong-Hoon Lee [a]

[a] *Department of Environmental Engineering, The University of Seoul, 90 Jeonnong-dong, Dongdaemun-gu, Seoul 130-173, South Korea*
[b] *Department of Maritime Environmental Engineering, Mokpo National Maritime University, 571-2 Chukkyo-dong, Mokpo, Cheonnam 530-729, South Korea*

Received 18 October 2006; received in revised form 8 March 2007; accepted 8 March 2007
Available online 14 March 2007

Abstract

The properties of dissolved organic matter (DOM) in the leachates discharged from lysimeters and landfill sites containing municipal solid waste incineration residues (MSWIRs) were studied. DOM samples were divided into hydrophobic acid, base, neutral (Hpo-A, Hpo-B, Hpo-N) and hydrophilic (Hpi) fractions using the fractionation method employing DAX-8 resin. Hpi was the smallest fraction of all the raw leachate samples. The proportion of Hpo-N increased with increasing operating time. Landfill sites containing abundant non-combustible wastes showed a higher proportion of Hpo-B than Hpo-A. The molecular weights and functional groups of the DOM fractions were studied by using gel permeation chromatography and FTIR, respectively. In addition, the fluorescent properties and binding sites of the DOM fractions were investigated using fluorescence analysis. In the synchronous scan spectra of each DOM fraction, most of DOM fractions showed an emission peak for the main fluorophores at around 300 nm or 350 nm, which are regarded as aromatic amino acid-like fluorophores. The interaction between the DOM fraction and the pollutants (Cu^{2+}, pyrene and phenanthrene) was investigated using the fluorescence quenching method. It was observed that the aromatic amino acid-like fluorophores in the DOM fractions could be an important factor affecting complexation with the pollutants.

Keywords: DOM fractions; DAX-8 resin; Synchronous scan specta; Fluorescence quenching

1. Introduction

Dissolved organic matter (DOM), which is ubiquitous in the environment, shows various properties in relation to its origin. Many studies have been carried out to characterize the physicochemical properties of DOM derived from different origins [2,3,8,10]. Dissolved humic substances (DHS), a major class of DOM usually show colloidal properties, e.g. a large surface area, mobility and an electronic double layer etc. [11]. For this reason, DOM has a wide range of molecular weights and sizes, ranging from a few hundred to hundreds of thousands of Daltons. Moreover, a number of functional groups in DOM, such as carboxylic, phenolic and carbonyl etc. allow them to interact with various substances in the environment [11].

A number of analytical methods exist for the investigation of DOM according to the various properties exhibited [6]. Since each method is limited to collecting precise information about DOM, a number of previous studies have synthetically examined the properties of DOM through various results obtained from different analytical methods.

A DOM fractionation method using resin adsorption has generally been applied in a number of studies [3,10,19]. Although the fractionation method provides meaningful information about DOM, it is also time consuming and labor intensive [7]. However, optical analysis rapidly provides useful information compared to fractionation methods. Fluorescence analysis especially can provide not only general properties of DOM, but information about reactivity with the various substances also (e.g. heavy metals, POPs, persistent organic pollutants) [5,21].

The reason DOM is important in the environment is a known significant factor, as it affects the behavior of the pollutants by redox reaction and hydrophobic/hydrophilic sorption rather than

* Corresponding author. Tel.: +82 61 240 7321; fax: +82 61 240 7284.
E-mail address: yjkim@mmu.ac.kr (Y.-J. Kim).

0304-3894/$ – see front matter © 2007 Elsevier B.V. All rights reserved.
doi:10.1016/j.jhazmat.2007.03.027

being a contaminant itself [3,16]. In particular, DOM derived from the decomposition of solid waste can affect the entire existence (extraction, transmission, degradation) of the pollutants in landfill sites. Since the composition of solid waste (as a source of DOM) in landfill sites varies greatly, it is very hard to recognize certain properties of DOM in relation to its origins, and sufficient studies have not been carried out comparing the origins of DOM (lake, peat, soil, river etc.).

Landfill sites are artificial places, which contain higher concentrations of DOM and pollutants than any other natural environments; therefore, their proper management must consider the interactions between DOM and pollutants.

The South Korean government set a goal for the gradual increase in the incineration rate of domestic solid wastes up to 30% by the year 2011. Therefore, the generation of incineration residues (fly ash and bottom ash were 64,713 tonnes and 315,334 tonnes, respectively, in 2004) would be expected to constantly increase. In South Korea, most incineration residues are reclaimed with domestic solid wastes.

Solid waste incineration residues contain significant amounts of heavy metals and persistent organic pollutants (POPs, e.g. dioxins, polycyclic aromatic hydrocarbons (PAHs), etc.); with the finer fly ash showing higher concentrations than bottom ash, which generally undergoes a stabilization/solidification process before landfill. However, bottom ash can be reclaimed with other wastes without pretreatment. Even though bottom ash shows less leachabilities of the pollutants than fly ash, the quantities of leachable pollutants from bottom ash are still considerable due to the large amounts generated compared to fly ash. Schramm et al. [22] reported that PCDDs/DFs (polychlorinated dibenzo-*p*-dioxins and polychlorinated dibenzo furans) in fly ash could easily be eluted with water containing surfactants, such as linear alkylbenzene sulfonate (LAS). Also, Kim et al. [15] reported that humic substances enhanced the leachabilities of PCDDs/DFs from incineration residues.

The release of metals from incineration residue is affected by three different factors; these being, dissolution of minerals (solubility control) [28], adsorption processes (sorption control) [28] and its availability (or total content) [28,29] in the incineration residue. Some metals contained within incineration residues will have relatively higher concentrations than others (e.g. Cu^{2+}) not controlled by the dissolution of minerals, but these will often be controlled by adsorption to the DOM surfaces [28]. There have been a number of studies on the reactivity of Cu^{2+} with organic carbon (humic acid, fulvic acid etc.) (e.g. [21,30]). Wu et al. [30] reported that the solubility of Cu^{2+} in solution was enhanced by the chelating interaction with humic substances. As outlined above, DOM plays an important role in the leaching of pollutants from incineration residues; however, the physicochemical diversity of DOM often causes interpretative difficulties. Hence, many properties of DOM, including interaction with the pollutants, are still being investigated, even though many studies have previously been performed.

The aims of this study were to characterize the DOM in leachate discharged from lysimeters and landfill sites containing MSWIRs, using the fractionation method, and examine the interaction between the DOM fractions and Cu^{2+}, as an inorganic pollutants, and pyrene and phenanthrene, two PAHs, as organic pollutants, using fluorescence analysis.

2. Materials and methods

2.1. Sample collection

Raw leachate samples were collected from 2 lysimeters and 12 landfill sites containing MSWIRs.

The cylinder type (diameter: 1 m, height: 5 m) lysimeters (LM1 and LM2) have been operated under the same operating conditions since May 2005. LM1 contained readily degradable waste such as sewage sludge (11%) and food waste (24.2%), while LM2 contained abundant barely degradable waste such as vinyl plastic (19.6%) and wood (12.9%) etc. and more non-combustible wastes (39.4%) than LM1. LM1 samples collected three times at regular intervals (operating period of LM1a: 0.6 year, that of LM1b: 0.8 year, that of LM1c: 1 year) to investigate the influence of operating period on the properties of DOM.

Landfill site samples were obtained from 12 sites which show a variety of operating periods, landfill areas and leachate generation as shown in Table 1. The main reclaimed wasted type was municipal solid waste (MSW) in most of landfill sites. However, L-2 and L-8 contained abundant amounts of non-combustible wastes compared to the other sites (more than 80% of total reclaimed wastes). A control site (L-12), which contained mainly incineration residues, was chosen for comparison with the other sites.

L-3 and L-9 are individual landfill sites located in the same wide landfill area. Although they are operated individually, their leachates are treated together. Besides the raw leachate, treated leachate (L-13) was also obtained from the leachate treatment plant, where the influent was a 1:1 mixture of raw leachate samples of L-3 and L-9. The process of leachate treatment plant consists of a series of four-functional unit (influent volume equalization – nitrification/denitrification – coagulation/precipitation – fenton oxidation).

The general characteristics of the lysimeters and landfill sites are shown in Table 1.

2.2. DOM fractionation

All samples were filtered through a GF/B glass-fiber filter (Whatman, 1.0 μm). Sample filtrates were diluted with deionized water until the TOC was less than 500 ppm.

One hundred grams (dry weight) of the DAX-8 resin (Sigma–Aldrich Co.), cleaned and conditioned as described by Thurman and Malcolm [25], was packed into a glass column (ID: 3 cm), rinsed alternately with 0.1 M-NaOH and 0.1 M-HCl until the TOC of each eluent was 0 ppm, and then rinsed with deionized water until the TOC of eluent was 0 ppm, prior to sample injection. After a final rinse, 200 mL of diluted sample was injected into the column.

The samples were fractionated into four fractions, i.e. hydrophobic acid (Hpo-A), hydrophobic neutral (Hpo-N), hydrophobic base (Hpo-B) and hydrophilic fraction (Hpi) using the fractionation method. Elution with 50 mL 0.1 M-HCl and

Table 1
The general characteristics of lysimeters and landfill sites

Site	Operating period (year)[a]	Landfill area ($10^3 m^2$)	Leachate amount (m^3 day^{-1})	Reclaimed waste type[b]	Remarks
LM1[c]	1	Diameter: 1 m,	-	MSW, MSWIR	Cylinder type
LM2[d]		Height: 5 m		MSW, IW, MSWIR	
L-1	0–1	338	200	MSW, IW, MSWIR	
L-2[e]	3–4	41	40	MSW, MSWIR	
L-3	4–5	3700	1691	MSW, IW, BW, MSWIR	
L-4	5–6	155	100	MSW, BW, MSWIR	
L-5	7–8	404	380	MSW, MSWIR	
L-6	8–9	321	1236	MSW, MSWIR	Closed
L-7	11–12	142	150	MSW, MSWIR	
L-8[f]	12–13	163	380	MSW, IW, MSWIR	
L-9	13–14	4100	2217	MSW, IW, BW, MSWIR	Closed
L-10	14–15	279	365	MSW, MSWIR	Closed
L-11	15–16	585	750	MSW, IW, MSWIR	
L-12	4–5	47	100	MSWIR	Control site

[a] The basic year (landfill site: July 2005, lysimeter: May 2006).
[b] MSW: municipal solid waste, MSWIR: municipal solid waste incineration residue, IW: industrial waste, BW: bulk waste.
[c] LM1: combustibles 80.2% (including food waste: 24.2%, sewage sludge: 11%), non-combustibles 19.8%.
[d] LM2: combustibles 60.6% (including vinyl plastic: 19.6%, wood: 12.9%), non-combustibles 39.4%.
[e] L-2: non-combustibles 70–80%, MSWIR 10%.
[f] L-8: construction waste 16%, MSWIR 77%.

0.1 M-NaOH were carried out until no TOC was detected. At this time, the elution rate was 3 mL min^{-1}.

The TOC of each DOM fraction was measured using a TOC analyzer (TOC-5000A, Shimadzu Co.). Each DOM fraction was calculated as follows:

$$\text{Hpo-A} = \text{DOM3} \times (\text{elutant volume}/200\,\text{mL})$$
$$\text{Hpo-B} = \text{DOM2} \times (\text{elutant volume}/200\,\text{mL})$$
$$\text{Hpi} = \text{DOM4} \times (\text{elutant volume}/200\,\text{mL})$$
$$\text{Hpo-N} = [\text{DOM1}] - [\text{Hpo-A}] - [\text{Hpo-B}] - [\text{Hpi}]$$

where the injected sample volume was 200 mL and [DOM1]–[DOM4] are as shown in Fig. 1, indicating the scheme of DOM fractionation.

Additional analyses (molecular weight, functional group, synchronous scan, binding site analysis) of each DOM fraction were carried out after fractionation. The pH of each DOM fraction was readjusted to between 7 and 8 with 1 M-HCl and 1 M-NaOH prior to the next analyses with the exception of functional group analysis using FTIR.

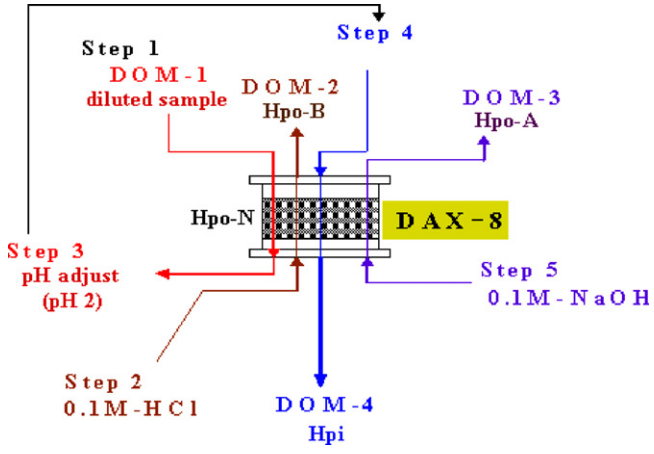

Fig. 1. The scheme of DOM fractionation.

2.3. Molecular weight analysis

Gel permeation chromatography (GPC) was performed to analyze the molecular weight distribution of each DOM fraction.

The analytical conditions were as follows:

- column: Shodex SB-802.5 HQ;
- flow rate/wavelength: 1 mL min^{-1}/254 nm;
- solvent: water (J.T. Baker, HPLC grade);
- molecular weight standards: polyethylene glycol (0.6 kDa, 1 kDa, 2 kDa, 6 kDa);
- operation software**:** Class-vp ver.6.14/GPC for Class-vp ver.1.03 (Shimadzu Co.).

2.4. Optical instrument analysis

The IR spectrum of each fraction was collected from FTIR (IRPrestige-21, Shimadzu Co.) employing MIRACLE (Zn Se prism Shimadzu Co., liquid state analysis device). Fluorescence analysis was performed using a fluorescence spectrophotometer (RF5301-PC Shimadzu Co.). A synchronous scan (Sys) was carried out on each DOM fraction, with the Sys spectrum collected in the 230–530 nm excitation wavelength range using a bandwidth of $\Delta\lambda = 20$ nm between the excitation and emission monochromator at a scan speed of slow mode (slits width for both excitation and emission were 5 nm). Before processing of the fluorescence spectral data, the background spectrum; deionized water with the pH adjusted to 7–8 with 0.1 M-HCl or 0.1 M-NaOH, was subtracted. The fluorescence intensity of each sample was divided by organic carbon concentration (ppm) of each sample. The effects of scattered light and Raman scattering were negligible in the all of samples. No corrections for fluctua-

tion of instrumental factors and absorption effects (e.g. primary and secondary inner filter effects) were applied to obtained fluorescence data since all of experiments were carried out under the same instrumental conditions and samples were diluted fully [2,13,17].

2.5. Binding site study

Each DOM fraction (30 mL) was passed through 30 mL (wet volume) of strong cation exchange resin (Dowex HCR-W2, H^+ form), which was packed into a glass column (ID: 1.5 cm) to free up the DOM binding sites. The pH of the eluent was adjusted to between 7 and 8 using 1 M-HCl and 1M-NaOH.

Stock solutions of Cu(II), pyrene and phenanthrene were prepared to investigate the interactions of each DOM fraction with pollutants. A 0.1 M of Cu(II) stock solution was prepared using reagent grade $CuCl_2{\cdot}2H_2O$.

Pyrene and phenanthrene stock solutions were prepared by dissolving 1 mg of pyrene and 19 mg of phenanthrene in 2 mL of benzene, respectively. Each solution was stirred sufficiently under N_2 gas. In the meantime, solvent of stock solutions were exchanged from benzene into methanol. After solvent conversion, the total volume of each stock solution was adjusted to 30 mL with methanol.

0.3 mL of 1 mg pyrene/30 mL MeOH and 1 mL of 19 mg phenanthrene/30 mL MeOH were added to a 1 L volumetric flask with 1 L of deionized water. Each aqueous stock solution was then shaken for over 24 h at 45 °C to minimize the methanol content in the aqueous stock solution. After stock solution preparation, the fluorescence quenching analysis was carried out. 3.5 mL of each DOM fraction was prepared in a non-fluorescent cell. After the addition of titrant (1 μL of Cu^{2+} stock solution) into the cell, the solution was stirred for 5 min using a small magnetic bar placed in the cell, and the Sys spectrum then collected under the same conditions ($\Delta\lambda = 20$ nm, emission range: 250–550 nm) used in the Sys analysis. The above titration procedure was carried out until the intensity at the maximum quenching wavelength was no longer quenched.

In contrast to the Cu^{2+} titration, 3.5 mL of pyrene and phenanthrene stock solutions were prepared in non-fluorescent cells, with 1 μL of each DOM fraction added to the cell as the titrant. After stirring the solution for 5 min to make an equilibrium based on [5], the synchronous scan spectrum was collected. The above titration procedure was carried out until the intensity at the intrinsic emission wavelength for pyrene (374 nm) and phenanthrene (366 nm) was no longer quenched. The above experiments were carried out at room temperature, with the pH maintained within 7–8 during the titration.

Interactions between the DOM fractions and pollutants were examined by using the Stern–Volmer equation which representatively describes static/collisional quenching among the various quenching mechanisms [17].

The Stern–Volmer equation can be represented as follow:

$$\frac{F_0}{F} = 1 + K[Q] \tag{1}$$

where F_0 and F are the initial intensity of the ligand solution without and with a quencher, respectively. K is the static or collisional quenching constant, and Q the total concentration of quencher. The Stern–Volmer equation assumes that all the fluorophores contact with the quencher. In some cases, the Stern–Volmer plot will display downward curvature, which presupposes two fluorophore populations, one being accessible (a) to quenchers, and the other not or buried (b) [17]. The existence of two fluorophore populations causes deviations from linearity in Eq. (1). Hence, K can be calculated using a modified Stern–Volmer equation for describing two fluorophore populations.

The following describes modified Stern–Volmer equation:

$$\frac{F_0}{\Delta F} = \frac{1}{(fK[Q])} + \frac{1}{f} \tag{2}$$

where $\Delta F = F_0 - F$, and f is the fraction of the initial fluorescence accessible to the quencher. Hence, f can be expressed as follow:

$$f = \frac{(100 - I_{res})}{100} \tag{3}$$

As shown in Eq. (3), I_{res} (residual intensity) refers to either the percentage of fluorophores not participating in complexation (maximum initial intensity is regarded as 100%) or the percentage inaccessible to the quencher.

3. Results

3.1. Characteristics of leachate samples

The general characteristics of each sample are summarized in Table 2. The pH of the leachate samples ranged from 6.3 to 8.13. Since the pH of every sample was under 8.3, the alkalinity of each sample might have been due to bicarbonate; a large amount of mineral species are also expected to exist in the leachate as the bicarbonate form.

As shown in Table 2, LM1 samples showed a sudden decrease in some parameter values (COD_{cr}, BOD, TOC, SS) with increasing of operating period.

At the landfill sites, the concentration of total solids ranged from 0.28 to 1.55%. Fixed solid was a major fraction of the total solids in all the landfill site samples, implying that inorganic colloids account for a large part of the total solids. The two landfill sites (L-1 and L-4), which have high BD, showed the highest proportion for VSS; conversely, treated leachate (L-13) showed the lowest proportion for VSS and highest proportion for FS. Even though the operating period of L-12 was short, its BD was as low as the L-11, which is the eldest landfill site; its OCF was also the lowest.

3.2. Distribution of DOM fractions

3.2.1. Lysimeter samples

The distribution of the DOM fractions in the lysimeter samples as well as the concentration change of each DOM fraction of the LM1 samples are shown in Fig. 2a and b, respectively. In all cases, the hydrophobic fraction was higher than the hydrophilic

Table 2
The general characteristics of leachate samples

Sample	pH	Alkalinity	mgL^{-1}			BD[a]	OCF[b]	Solids %			
		(mgL^{-1} as $CaCO_3$)	COD_{cr}	BOD	TOC			VDS	VSS	FS	TS
LM1a	6.30	18,280	90,667	80,850	25,260	0.89	0.28		SS: 5077 mgL^{-1}		
LM1b	7.65	12,480	35,200	28,087	13,536	0.80	0.38		SS: 1400 mgL^{-1}		
LM1c	7.74	12,460	5,200	1,898	1,514	0.37	0.29		SS: 750 mgL^{-1}		
LM2	7.54	-[c]	-	-	1,314	-	-		SS: 550 mgL^{-1}		
L-1	6.81	1,520	3,460	2,420	1,877	0.70	0.54	0.15 (28)[d]	0.07 (14)	0.30 (58)	0.52
L-2	7.27	4,600	520	217	649	0.42	1.25	0.09 (18)	0.02 (4)	0.39 (78)	0.51
L-3	7.53	5,420	4,000	2,190	1,591	0.55	0.40	0.19 (12)	0.05 (3)	1.31 (84)	1.55
L-4	7.71	5,360	1,360	1,323	944	0.97	0.69	0.05 (10)	0.07 (14)	0.37 (77)	0.49
L-5	8.13	12,000	1,440	650	1,783	0.45	1.24	0.18 (19)	0.04 (4)	0.72 (77)	0.93
L-6	7.57	5,000	2,500	1,140	1,534	0.46	0.61	0.06 (10)	0.08 (13)	0.48 (77)	0.63
L-7	7.32	4,620	660	420	751	0.64	1.14	0.07 (16)	0.02 (4)	0.36 (79)	0.45
L-8	7.24	1,260	300	164	248	0.55	0.83	0.02 (8)	0.01 (2)	0.25 (90)	0.28
L-9	8.01	7,800	1,600	690	1,169	0.43	0.73	0.11 (13)	0.03 (4)	0.75 (84)	0.90
L-10	7.79	2,840	900	570	472	0.63	0.52	0.05 (12)	0.01 (3)	0.31 (84)	0.37
L-11	7.58	8,800	3,600	720	2,234	0.20	0.62	0.18 (18)	0.04 (4)	0.78 (78)	1.00
L-12	6.87	3,000	840	183	190	0.22	0.23	0.04 (11)	0.01 (2)	0.31 (86)	0.36
L-13	7.79	2,840	360	136	141	0.38	0.39	0.07 (6)	0.01 (1)	1.10 (93)	1.18

[a] BD: biodegradability, BOD/COD_{cr}.
[b] OCF: oxidized organic carbon fraction in COD_{cr}, TOC/COD_{cr}.
[c] No data.
[d] Percentage of each solid fraction in total solids.

fraction. Hpo-A was the predominant fraction in LM1 samples, while Hpo-N was dominant in the LM2 samples. The proportion of Hpo-B in all the samples was similar (25.8–29.1%). In LM1 samples, the proportion of Hpo-N increased with increasing operating period. Although LM1c and LM2 have same operating period, the proportion of Hpo-N at LM2 was greater than that at LM1c, and that of Hpo-B in LM2 was similar to that of Hpo-A. In Fig. 2b, the slope for Hpo-A was the sharpest. Although the

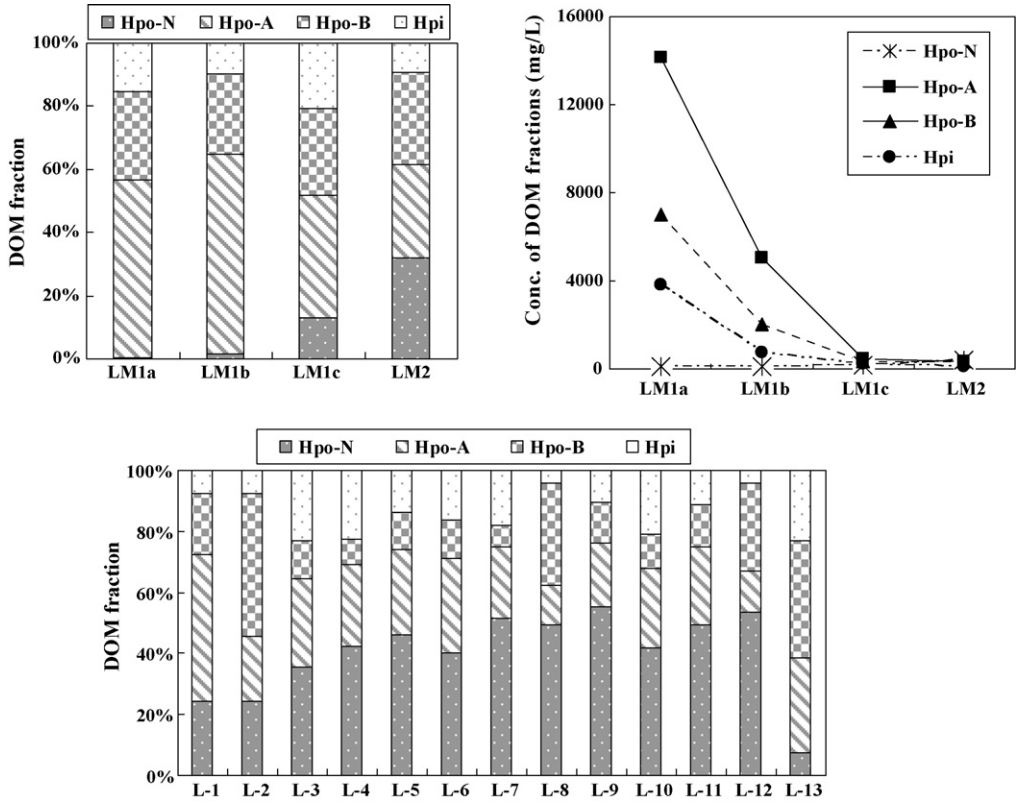

Fig. 2. Distribution of DOM fractions in lysimeter samples (a, top left) and in landfill site samples (c, bottom), concentration change of each DOM fraction of LM1 samples (b, top right).

Table 3
The molecular weight and polydispersity of each DOM fraction

Sample		M_w[a]	M_n[b]	D[c]	Sample		M_w	M_n	D
LM1a	Hpo-A	22,968	18,323	1.254	L-6	Hpo-A	4604	3578	1.287
	Hpo-B	3,714	2,988	1.243		Hpo-B	1296	1288	1.006
	Hpi	3,079	3,075	1.001		Hpi	1277	1272	1.004
LM1b	Hpo-A	19,961	16,131	1.237	L-7	Hpo-A	5336	4305	1.239
	Hpo-B	2,243	2,202	1.019		Hpo-B	1276	1267	1.007
	Hpi	2,244	2,214	1.014		Hpi	1241	1235	1.005
LM1c	Hpo-A	15,815	12,207	1.296	L-8	Hpo-A	4002	3189	1.255
	Hpo-B	2,716	2,449	1.109		Hpo-B	1348	1341	1.005
	Hpi	2,910	2,887	1.008		Hpi	1454	1447	1.005
LM2	Hpo-A	10,467	6,246	1.676	L-9	Hpo-A	6047	3935	1.537
	Hpo-B	2,513	2,284	1.100		Hpo-B	1611	1607	1.002
	Hpi	2,793	2,519	1.109		Hpi	1666	1657	1.005
L-1	Hpo-A	3,866	2,040	1.895	L-10	Hpo-A	4388	3603	1.218
	Hpo-B	1,350	1,330	1.015		Hpo-B	1232	1227	1.004
	Hpi	1,819	1,579	1.152		Hpi	1214	1207	1.006
L-2	Hpo-A	4,560	1,887	2.417	L-11	Hpo-A	6047	4420	1.368
	Hpo-B	1,866	1,352	1.380		Hpo-B	1446	1442	1.003
	Hpi	1,863	1,370	1.360		Hpi	1612	1606	1.004
L-3	Hpo-A	4,165	3,356	1.241	L-12	Hpo-A	4859	4089	1.188
	Hpo-B	1,545	1,542	1.002		Hpo-B	2130	1480	1.439
	Hpi	1,678	1,651	1.016		Hpi	1820	1480	1.230
L-4	Hpo-A	5,643	4,523	1.248	L-13	Hpo-A	7746	2824	2.743
	Hpo-B	1,310	1,305	1.004		Hpo-B	2236	2115	1.057
	Hpi	1,264	1,259	1.004		Hpi	1524	1393	1.094
L-5	Hpo-A	4,655	2,287	2.035					
	Hpo-B	1,485	1,478	1.005					
	Hpi	1,752	1,486	1.179					

[a] Weight-average molecular weight (Dalton).
[b] Number-average molecular weight (Dalton).
[c] Polydispersity (M_w/M_n).

proportion of Hpo-N increased with increasing operating period, the concentration changes of it were insignificant.

3.2.2. Landfill site samples

The distribution of the DOM fractions is shown in Fig. 2c. As for the lysimeter samples, the hydrophobic fraction was higher than the hydrophilic fraction. Hpo-A was dominant compared to Hpo-B in most of the samples with the exception of L-2, L-8 and L-12, which contained abundant amounts of non-combustible wastes, and the L-13 treated leachate sample. Hpo-N generally increased with increasing operating period; nevertheless, L-12 has only been operating for a short period, but the proportion of Hpo-N was as high as that of L-11. L-13 showed the highest proportion of Hpi, but the lowest proportion of Hpo-N.

3.3. Molecular weight and polydispersity

The results and typical chromatograms obtained from the GPC analysis are shown in Table 3 and Fig. 3, respectively.

In LM1, the weight-average molecular weight (M_w) of Hpo-A decreased with increasing operating period. In comparison with LM1c and LM2, which have the same operating period, the M_w of each DOM fraction in LM2 was a little lower than that in LM1c. For the results of the landfill sites, the M_w of Hpo-A ranged from 3866 to 7746 Da; however, those of Hpo-B and Hpi were within similar ranges, and less than 2,300 Daltons. The M_w of Hpo-A was higher than those of Hpo-B and Hpi in all the samples. With the exception of the control site (L-12), the polydispersity of Hpo-B and Hpi were close to 1.0 in all the samples, indicating that the molecular weight distribution range was narrow, namely Hpo-B and Hpi consisted of monodispersed compounds; however, the polydispersity of Hpo-A was higher than 1.0.

3.4. Functional group analysis

There were no significant differences in the IR spectra between the same DOM fractions with operating period or type of waste buried; hence, a representative IR spectrum of each DOM is shown in Fig. 4.

The IR spectrum of each DOM fraction was dominated by two peaks; 3400–3300 cm^{-1} related to carboxylic, alcoholic, phenolic O–H stretching, and at 1725–1630 cm^{-1} related to carboxylic, ketonic, amid, quinone C=O stretching, respectively. However, the Hpo-A fraction showed an additional peak at around 1400 cm^{-1}, which was expected to be due to

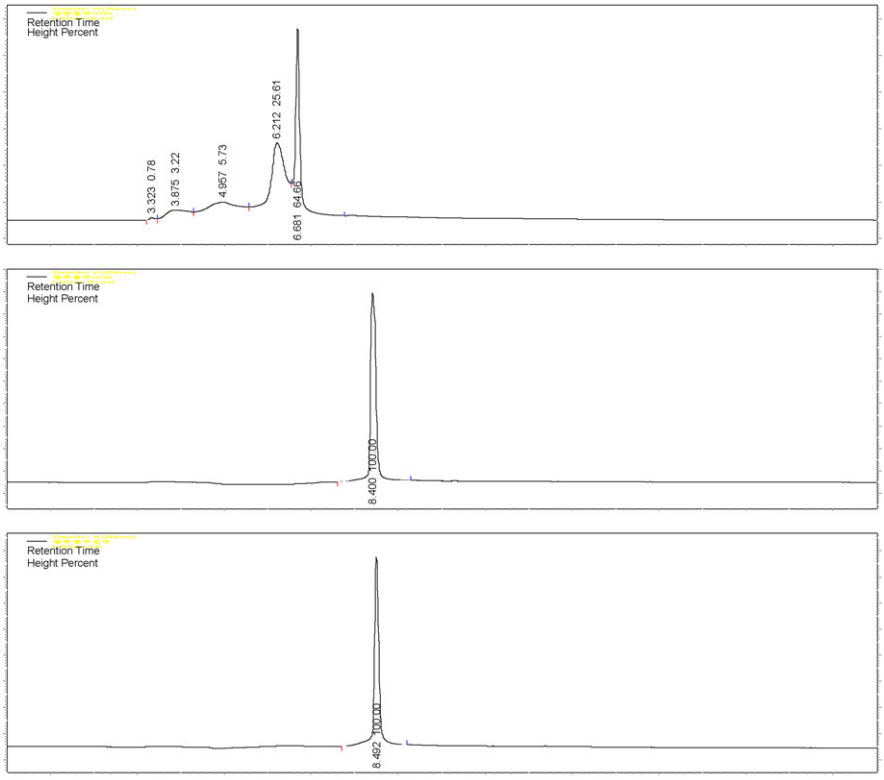

Fig. 3. Typical chromatograms (L-4) for the molecular weight analysis (top: Hpo-A, middle: Hpo-B, bottom: Hpi).

the deformations of aliphatic C–H and phenolic OH groups [20].

3.5. Synchronous scan (Sys) spectrum

Sys spectra of the samples and their details are shown in Fig. 5 and Table 4, respectively.

3.5.1. Lysimeter

The fluorophores in the LM1 samples were inactive under the above mentioned analytical conditions ($\Delta\lambda = 20$, emission: 250–550 nm); hence, the Sys spectra of the LM1 samples were obtained using different analytical conditions ($\Delta\lambda = 40$, emission: 260–380 nm). As shown in Fig. 5, the LM1 samples showed common peaks at around 310 nm and 350 nm. The fluorescence intensity of each DOM fraction in the LM1 samples with the exception of Hpi of LM1c increased; Hpo-B and Hpi of the LM1 samples showed an additional peak at 325 nm with increasing operating period. There were marked differences in the analytical conditions ($\Delta\lambda$, emission range) and Sys spectra between the LM2 and LM1c samples, which both have the same operating period.

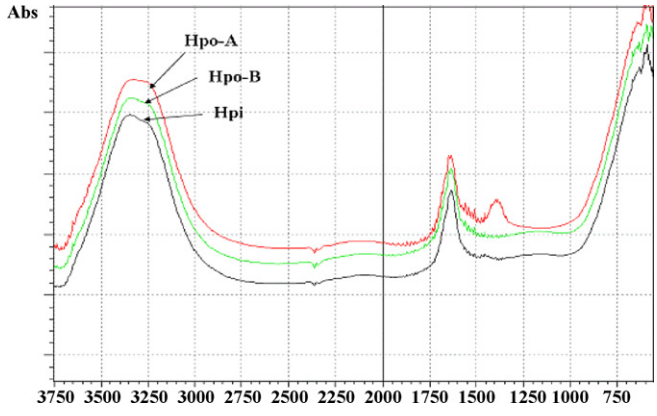

Fig. 4. IR spectrum of each DOM fraction.

3.5.2. Landfill site

In Fig. 5, the DOM fractions from the landfill sites showed various spectra shapes; moreover, spectrum peaks of most samples overlapped at longer wavelengths (over 300 nm); therefore, it was hard to precisely identify the fluorescent structure. However, each DOM fraction from the landfill sites commonly showed maximum intensities around 280/300 and 336/356, or 346/366 nm (excitation/emission).

The maximum intensities at L-1 for Hpo-A and at L-4 for Hpo-B, which showed high biodegradability (BOD/COD_{cr}), were the lowest, and for each DOM treated leachate (L-13) fraction with the exception of Hpo-A were the highest (Hpo-A was the second highest after L-9). As shown in Fig. 5, in contrast to other sites, all three DOM fractions of L-2 and L-8, which contained abundant amounts of non-combustible wastes, showed a dominant peak at around 356 nm compared with another peak at around 300 nm. The Hpo-A and Hpi of the control site (L-12) showed spectra with simple shapes compared to those of the other sites with all Hpo-B peaks found within 360 nm. A peak at around 500 nm was observed from many of the sites. Especially, Hpo-B of L-10, an old closed landfill site, showed a higher intensity than at the other sites in this region.

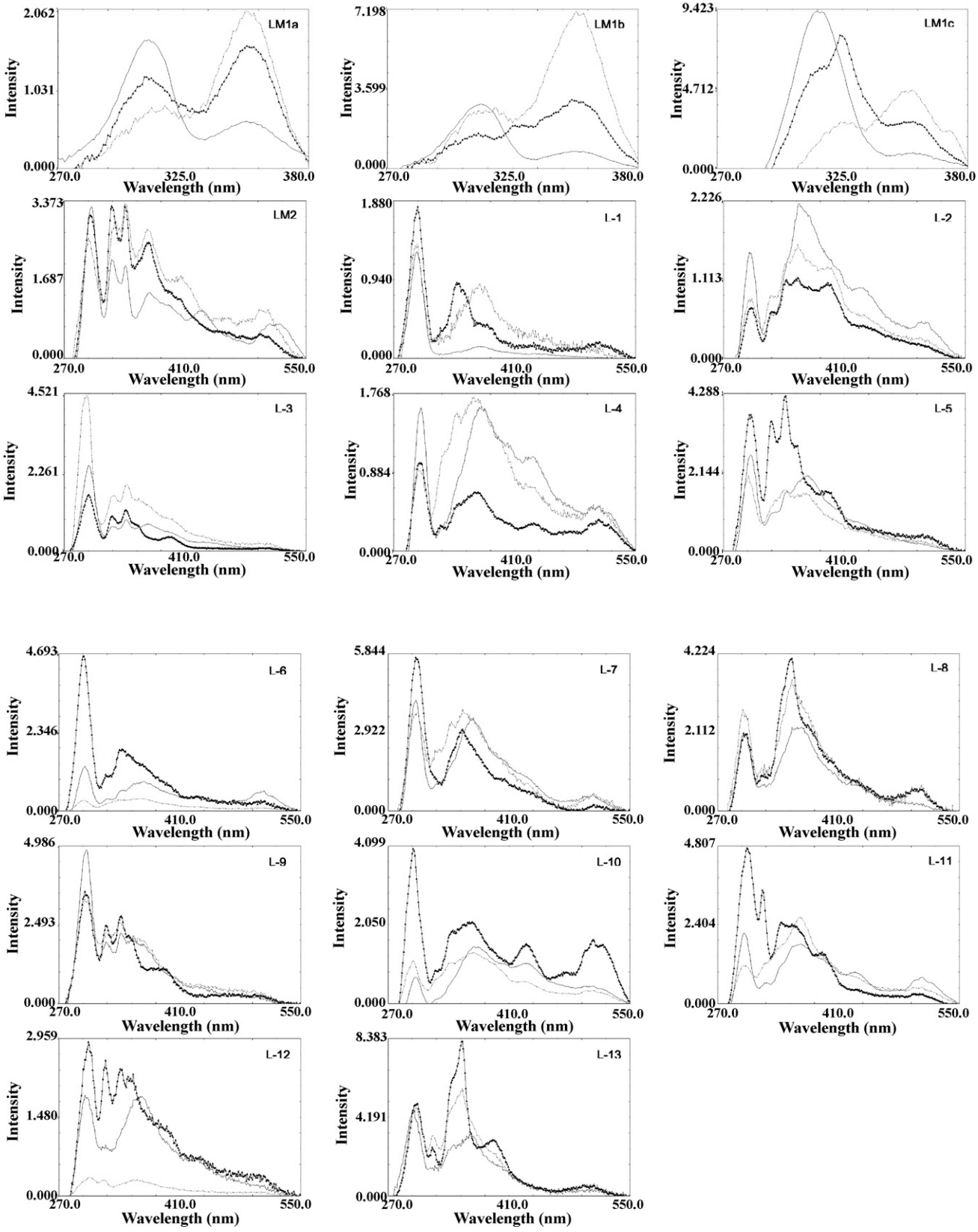

Fig. 5. Synchronous scan spectrum of each DOM fraction (Hpo-A: solid line, Hpo-B: triangle printed line, Hpi: dotted line).

Table 4
The summaries of synchronous scan spectra and binding site studies

		Synchronous scan data		Cu (II) titration results				Pyrene titration results				Phenanthrene titration results			
		exci/emi max. (Intensity)	Additional peak (exci/emi)	I_{res}[a] (nm)[b]	log K[c]	N[d]	r[e]	I_{res}	log K[c]	N	r	I_{res}	log K[c]	N	r
	Hpo-A	270/310 (1.669)	313/353	87.7 (308)	2.91 (4.22)[f]	8 (7)[f]	0.8802 (0.9881)[f]	82.6	3.56	5	0.9884	93.1	3.08	6	0.9747
LM1a	Hpo-B	313/353 (1.587)	268/308	90.7 (308)	3.02 (4.67)	5 (4)	0.8708 (0.9449)	82.1	4.05 (5.39)	5 (4)	0.9047 (0.9583)	88.6	3.65 (3.95)	6 (5)	0.9911 (0.9975)
	Hpi	313/353 (2.038)	270/310	48.3 (300)	4.05 (5.28)	5 (4)	0.7656 (0.8930)	82.3	4.27 (5.35)	5 (4)	0.8750 (0.9999)	88.2	3.65 (5.10)	10 (9)	0.9557 (0.9596)
	Hpo-A	271/311 (2.915)	312/352	83.9 (310)	2.94 (3.98)	9 (8)	0.9765 (0.9912)	81.6	3.98 (5.18)	4 (3)	0.9149 (0.9752)	94.6	3.35	4	0.9499
LM1b	Hpo-B	312/352 (3.110)	270/310	96.9 (353)	2.51 (3.85)	5 (4)	0.944 (0.9643)	81.6	4.42 (5.24)	5 (4)	0.9746 (0.9764)	96.6	3.74	4	0.9295
	Hpi	313/353 (7.115)	277/317	-[g]	-	-	-	80.5	5.79 (6.05)	5 (4)	0.8347 (0.9764)	97.1	5.4	2	1.0
	Hpo-A	274/314 (9.302)	316/356	70.8 (312)	3.09 (3.84)	14 (13)	0.9395 (0.9982)	85.3	4.16 (5.03)	4 (3)	0.9713 (0.9978)	93.4	3.65 (5.02)	5 (4)	0.9761 (0.9405)
LM1c	Hpo-B	284/324 (7.899)	316/356	79.2 (324)	3.10 (4.01)	11 (10)	0.8304 (0.9966)	88.5	4.20 (4.42)	4 (3)	0.9987 (0.9997)	95.9	3.53 (5.05)	5 (4)	0.9478 (0.8315)
	Hpi	316/356 (4.628)	284/324	54.9 (326)	3.96 (5.00)	5 (4)	0.7398 (0.9517)	87.4	4.46 (5.75)	5 (4)	0.9948 (0.9016)	91.6	4.19	5	0.9750
	Hpo-A	282/302 (3.247)	305/325, 321/341 350/370, 408/428 488/508	66.5 (300)	3.19 (3.56)	18 (17)	0.9914 (0.6670)	65.2	3.96 (4.83)	7.(6)	0.9471 (0.9732)	84.3	3.46 (4.37)	8 (7)	0.9798 (0.9699)
LM2	Hpo-B	305/325 (3.261)	280/300, 321/341 348/368, 278/298	7.34 (3.66)	3.30 (4.92)	9 (8)	0.6567 (0.9766)	80.0	3.92 (4.99)	6 (5)	0.9645 (0.8947)	88.7	3.62 (5.06)	7 (6)	0.9147 (0.9341)
	Hpi	320/340 (3.324)	346/366, 476/496	86.7 (366)	3.03 (4.47)	7 (6)	0.8133 (0.9947)	77.7	4.69 (5.89)	4 (3)	0.8897 (0.9769)	92.7	3.76	8	0.9797
	Hpo-A	270/290 (1.273)	349/369	53.2 (297)	3.38 (3.97)	15 (14)	0.9781 (0.9919)	74.6	3.45 (5.10)	8 (7)	0.3844 (0.9746)	94.1	2.93 (4.21)	4 (3)	0.9733 (0.7921)
L-1	Hpo-B	278/298 (1.809)	323/343	72.3 (298)	3.74 (5.23)	4 (3)	0.7643 (0.9989)	81.4	4.20 (5.35)	5 (4)	0.8212 (0.9877)	86.4	3.98 (4.88)	5 (4)	0.9703 (0.9938)
	Hpi	277/297 (1.363)	350/370	-	-	-	-	76.5	4.82 (6.07)	4 (3)	0.8373 (0.9725)	90.2	4.15	5	0.9979
	Hpo-A	337/357 (2.184)	280/300, 479/499	28.0 (300)	3.63 (3.83)	20 (19)	0.9833 (0.9809)	77.8	4.01 (6.01)	5 (4)	0.8042 (0.7603)	82.1	3.79 (4.87)	6 (5)	0.9389 (0.9902)
L-2	Hpo-B	336/356 (1.140)	283/303	73.5 (357)	3.51 (4.94)	6 (5)	0.6139 (0.9854)	90.7	3.31 (2.96)	5 (4)	0.9267 (0.9072)	90.0	3.49	4	0.9966
	Hpi	336/356 (1.612)	283/303	80.7 (356)	3.62 (5.86)	3 (2)	0.8778 (1.0)	71.9	4.31 (5.64)	5 (4)	0.8060 (0.8961)	87.1	3.87 (6.41)	5 (4)	0.4979 (0.9831)
	Hpo-A	279/299 (2.451)	304/324, 322/342 348/368	46.1 (299)	3.57 (3.76)	13 (12)	0.9807 (0.9987)	77.7	3.85 (4.85)	7 (6)	0.8924 (0.9785)	90.8	4.1	2	1.0
L-3	Hpo-B	278/298 (1.614)	306/326, 321/341 374/394	80.1 (298)	3.16 (4.32)	8 (7)	0.9027 (0.9904)	83.1	3.74 (5.29)	5 (4)	0.7836 (0.9082)	89.6	3.56 (3.52)	4 (3)	0.9921 (0.9947)
	Hpi	276/296 (4.457)	308/328, 322/342	91.5 (296)	3.00 (5.11)	5 (4)	0.6758 (0.8760)	81.3	4.34 (5.05)	4 (3)	0.9894 (0.9804)	91.4	3.81 (5.12)	6 (5)	0.8953 (0.9983)
	Hpo-A	282/302 (1.606)	349/369, 411/431 487/507	31.3 (301)	3.69 (3.66)	16 (15)	0.9967 (0.9995)	68.3	3.92 (4.84)	11 (10)	0.9314 (0.9548)	82.9	4.01 (4.67)	4 (3)	0.9888 (0.9645)
L-4	Hpo-B	282/302 (0.989)	304 /324, 344/364 412/432, 487/507	62.4 (299)	3.57 (3.97)	7 (6)	0.9875 (0.9912)	79.3	3.84 (4.91)	5 (4)	0.9495 (0.9785)	87.8	3.62 (4.82)	5 (4)	0.9096 (0.9971)
	Hpi	343/363 (1.729)	278/298, 487/507	-	-	-	-	76.4	4.31 (5.63)	6 (5)	0.8251 (0.9785)	86.8	4.19 (5.25)	4 (3)	0.9614 (0.9882)
	Hpo-A	282/302 (2.622)	323/343, 348/368	14.3 (302)	3.90 (3.68)	25 (24)	0.9788 (0.9975)	81.2	3.86 (4.50)	6 (5)	0.8876 (0.9693)	92.3	3.56	4	0.9869
L-5	Hpo-B	282/302 (3.713)	306/326, 322/342	72.5 (301)	3.25 (4.52)	10 (9)	0.7716 (0.9954)	78.8	4.42 (5.11)	5 (4)	0.9829 (0.9006)	92.3	4.03	4	0.9630
	Hpi	279/299 (2.050)	323/343	96.1 (298)	3.51 (5.01)	3 (2)	0.9090 (1.0)	84.4	4.32 (5.39)	4 (3)	0.9651 (0.8388)	87.3	4.16	4	0.9438
	Hpo-A	280/300 (1.332)	349/369, 410/430 487/50	53.9 (300)	3.39 (3.91)	14 (13)	0.9644 (0.9975)	73.3	4.07 (4.66)	6 (5)	0.9868 (0.9785)	89.6	3.35 (4.17)	9 (8)	0.8896 (0.9845)
L-6	Hpo-B	279/299 (4.625)	304/324, 323/343 409/429	71.4 (299)	3.10 (4.24)	14 (13)	0.7337 (0.9859)	70.3	4.60 (5.58)	6 (5)	0.9262 (0.9785)	88.6	3.92	6	0.9763
	Hpi	279/299 (0.321)	320/340	-	-	-	-	82.1	3.82 (5.20)	4 (3)	0.8698 (0.9982)	93.0	3.16	5	0.9929
	Hpo-A	282/302 (4.108)	348/368, 486/506	56.3 (300)	3.46 (3.95)	11 (10)	0.9858 (0.9957)	84.5	4.02 (3.52)	5 (4)	0.9421 (0.9884)	92.9	3.67 (5.09)	6 (5)	0.8583 (0.9922)
L-7	Hpo-B	282/302 (5.702)	336/356, 488/508	76.2 (356)	3.30 (5.43)	8 (7)	0.6283 (0.9517)	80.0	4.36 (4.91)	7 (6)	0.8865 (0.9719)	93.8	4.04 (5.06)	4 (3)	0.9834 (0.9998)
	Hpi	336/356 (3.785)	283/303, 323/343 488/508	83.2 (355)	3.64 (4.75)	11 (10)	0.5536 (0.8686)	84.0	4.77 (4.72)	4 (3)	0.9472 (0.9778)	91.9	4.30 (5.40)	5 (4)	0.9643 (0.9941)
	Hpo-A	336/356 (2.250)	283/303, 403 / 423	55.8 (299)	3.56 (3.83)	9 (8)	0.9904 (0.9988)	87.6	4.84 (4.23)	4 (3)	0.9676 (0.9877)	92.6	3.80 (5.21)	5 (4)	0.9529 (0.9319)
L-8	Hpo-B	336/356 (4.099)	280/300, 486/506	80.1 (354)	3.34 (4.75)	6 (5)	0.7268 (0.9982)	83.3	4.44 (5.63)	6 (5)	0.8632 (0.9718)	92.0	3.79	8	0.9651
	Hpi	336/356 (3.526)	279/299, 402/422 486/506	79.7 (355)	3.52 (4.54)	4 (3)	0.9521 (0.9984)	91.9	4.5	5	0.9479	88.3	4.42 (5.42)	6 (5)	0.9524 (0.9927)
	Hpo-A	282/302 (4.862)	305/325, 322/342 336/356	67.4 (301)	3.30 (4.09)	11 (10)	0.8275 (0.9873)	77.1	4.40 (4.45)	4 (3)	0.9991 (0.9996)	88.5	3.97 (5.20)	5 (4)	0.9320 (0.9983)
L-9	Hpo-B	280/300 (3.543)	305 /325, 322/342 371/391, 477/497	91.6 (301)	2.84 (4.05)	6 (5)	0.9686 (0.9873)	77.7	4.25 (5.07)	5 (4)	0.9821 (0.9472)	89.5	3.74 (4.96)	7 (6)	0.9543 (0.9886)
	Hpi	280/300 (3.320)	305/325, 320/340 475/495	81.3 (301)	3.30 (4.68)	6 (5)	0.7832 (0.9873)	84.0	4.51 (5.09)	4 (3)	0.9880 (0.9987)	93.3	4.00 (5.60)	5 (4)	0.8865 (0.9965)
	Hpo-A	349/369 (1.480)	282/302, 410/430 486/506	62.4 (369)	3.57 (4.36)	7 (6)	0.9685 (0.9860)	52.5	3.91 (4.76)	10 (9)	0.9580 (0.9407)	87.3	3.66 (3.79)	4 (3)	0.9960 (0.9979)
L-10	Hpo-B	279/299 (4.032)	344 /364, 410/430 488/508, 499/519	60.0 (518)	3.33 (3.81)	13 (12)	0.9815 (0.9960)	72.4	4.11 (5.01)	7 (6)	0.9680 (0.9318)	86.1	3.74 (4.94)	7 (6)	0.9371 (0.9650)
	Hpi	349/369 (1.334)	279/299, 488/508	56.4 (299)	3.28 (3.99)	18 (17)	0.9202 (0.9988)	69.2	3.79 (4.36)	6 (5)	0.9790 (0.9821)	92.1	3.16 (4.00)	6 (5)	0.9733 (0.9947)
	Hpo-A	280/300 (2.141)	346/366, 409/429 486/506	43.2 (506)	3.43 (3.83)	19 (18)	0.9653 (0.9988)	77.2	3.69	8	0.9623	78.7	3.31 (4.44)	15 (14)	0.9806 (0.9203)
L-11	Hpo-B	284/304 (4.742)	302/322, 324/344 479/499	61.2 (305)	3.15 (4.11)	19 (18)	0.8833 (0.9818)	76.6	4.32 (4.58)	4 (3)	0.9882 (0.9962)	88.6	3.65	6	0.9781

Table 4 (*Continued*)

		Synchronous scan data	Cu (II) titration results				Pyrene titration results				Phenanthrene titration results			
		exci/emi max. (Intensity)	Additional peak (exci/emi)	I_{res}[a] (nm)[b]	log K[c]	N[d]	r[e]	I_{res}	log K[c]	N	r	I_{res}	log K[c]	N	r
	Hpi	346/366 (2.624)	279/299, 488/508	-	-	-	-	83.0	3.81 (4.83)	7 (6)	0.9550 (0.9870)	93.0	3.50	5	0.9919
	Hpo-A	28/300 (1.895)	346/366	63.4 (301)	3.47 (4.03)	9 (8)	0.9387 (0.9952)	82.6	4.30 (5.57)	5 (4)	0.8577 (0.9741)	88.3	4.01 (5.58)	6 (5)	0.7712 (0.9787)
L-12	Hpo-B	284/304 (2.900)	304/324, 321/341 336/356	89.3 (304)	3.19 (3.62)	4 (3)	0.9700 (0.9856)	80.9	4.51 (5.49)	5 (4)	0.9359 (0.9332)	88.8	4.48 (4.72)	3 (2)	0.9997 (1.0)
	Hpi	284/304 (0.354)	304/324, 336/356	-	-	-	-	76.8	3.90 (4.87)	6 (5)	0.9483 (0.9713)	91.2	3.57 (3.50)	4 (3)	0.9993 (0.9995)
	Hpo-A	278/298 (4.568)	344/364	82.5 (298)	3.44 (4.28)	4 (3)	0.9518 (1.0)	86.5	4.90	3	0.9956	95.4	4.12 (4.49)	5 (4)	0.9968 (0.9983)
L-13	Hpo-B	336/356 (8.243)	284/304, 302/322 371/391	43.9 (356)	4.23 (5.54)	5 (4)	0.7513 (0.9887)	84.5	4.21	6	0.9814	91.0	4.25 (5.36)	4 (3)	0.9562 (0.9999)
	Hpi	336/356 (5.741)	282/302, 302/322	66.6 (355)	3.77 (4.97)	6 (5)	0.8722 (0.8816)	91.4	4.19 (4.27)	6 (5)	0.9635 (0.9865)	-	-	-	-

[a] Residual intensity (% unit).
[b] Maximum quenched wavelength.
[c] Logarithm of the quenching constants (unit: M^{-1} for Cu^{2+}, L/mg for PAHs).
[d] The number of plots which were used to calculate log K.
[e] Correlation coefficient.
[f] log K, N and r, obtained from modified Stern–Volmer equation.
[g] No data (quenching was not observed).

3.6. Binding site studies

The Cu(II), pyrene and phenanthrene titration results are summarized in Table 4.

3.6.1. Cu(II) titration results

Compared with the lysimeter samples (LM1a, LM1b, LM1c), the residual intensities (I_{res}) of Hpo-A and Hpo-B decreased with increasing operating period; however, the I_{res} of Hpi increased in opposition to those of Hpo-A and Hpo-B. Compared with LM1c and LM2, LM1c showed higher I_{res} of Hpo-A and Hpo-B than LM2, but LM2 showed higher I_{res} of Hpi than LM1c. Also, the maximum quenched wavelengths of Hpo-B and Hpi in LM2 samples were relative longer (366 nm) than those in LM1c samples (324 nm and 326 nm).

In comparison with the landfill sites, an increasing trend in I_{res} i.e. Hpo-A < Hpo-B and Hpi, was observed at most landfill sites with few exceptions (especially L-13).

The r values (correlation coefficients) for Hpo-B and Hpi from the Stern–Volmer equation were generally lower than that for Hpo-A. Since the Stern–Volmer plots of Hpo-B and Hpi deviated from linearity, the Cu(II) titration data were treated using the modified Stern–Volmer equation. As shown in Table 4, the r values from the modified Stern–Volmer equation showed a better linear correlation. Compared with the log K of the DOM fractions in each sample obtained using the modified Stern–Volmer equation, Hpo-A showed an overall lower log K value than Hpo-B and Hpi.

3.6.2. PAHs titration results

As shown in Table 4, the I_{res} of pyrene and phenanthrene were more than 70% with the exception of a few samples. The I_{res} of pyrene and phenanthrene for each DOM fraction for LM2 were lower than for LM1c with the exception of Hpi for LM2 in the phenanthrene titration results.

At the landfill sites, the lowest I_{res} of pyrene for each DOM fraction can be found for those samples from closed landfill sites (Hpo-A and Hpi of L-10 and Hpo-B of L-6, respectively). There were no significant differences between the r values obtained using the Stern–Volmer plots or modified Stern–Volmer plot that were greater than those for the Cu(II) titration results with the exception of a few samples.

Pyrene showed higher log K and lower I_{res} values than phenanthrene for each DOM fraction. As shown in Table 4, the log K and I_{res} values showed various ranges for both pyrene and phenanthrene; hence, the comparison of one sample with another was difficult.

4. Discussion

4.1. The factors which can affect the distribution of DOM fractions

As shown in Fig. 2c, the proportion of Hpo-N roughly increased with increasing operating period. Also, a similar trend for Hpo-N was observed in Fig. 2a (LM1); however, according to Fig. 2b, the increase of Hpo-N was due to the concentration

decrease of the other DOM fractions. Therefore, it seems reasonable to assume that the increase in Hpo-N with increasing operating period is not due to a concentration increase, but to an increase in the relative proportion due to a decrease in the concentration of the other DOM fractions.

As reported in Section 3.2, both a lysimeter (LM2) and the landfill site (L-2, L-8, L-12) containing abundant amount of non-combustible wastes showed higher fractions of Hpo-N and Hpo-B. Besides, L-13 showed a quite different distribution trend of DOM fractions (lowest Hpo-N, highest Hpi), which was probably due to the influence of the leachate treatment process.

A previous study on the DOM from raw sewage and various kinds of wastewater treatment effluent reported that the proportion of hydrophilic DOM exceeded that of hydrophobic DOM [10]. Christensen et al. [3] suggested that the hydrophilic fraction accounted for about 30% of the DOM in groundwater polluted by landfill leachate.

Judged from this work and the above references, the operating period (time) and type of waste buried (as a source of DOM) could be important factors. However, other factors to affect the distribution of DOM fractions would also exist (e.g. treatment process type).

4.2. Physicochemical properties of DOM fractions

The DOM fractionation method employing DAX-8 resin is based on the ionization of acidic functional groups, which H-bond with the resin functional group (ester–oxygen) at a given pH (hydrophilic effect). It is well known that carboxylic and phenolic groups are most typically found in DOM [11,26,27]. As shown in Fig. 4, the IR spectra of each DOM fraction were in accordance with the previous studies referenced above. The Hpo-A eluted by the ionization of phenolic functional groups, as observed from the IR spectrum at around 1400 cm^{-1}, can be regarded as an amphiphilic fraction because it can be retained in the resin, even when the acidic sites are ionized by 0.1 N-HCl elution [18]. Hpo-N, which was not eluted due to the hydrophilic effect but retained in resin can be regarded as more hydrophobic than the other fractions.

Imai et al. [10] reported that organic compounds such as aromatic amines were often found in Hpo-B; also the absence of Hpo-B has been reported in both lake and river waters. They also reported that Hpi was considered to include carbohydrate-like DOM (Hpi-N), proteins and amino acids (Hpi-B). Hydrocarbons, pesticides, carbonyl compounds and synthetic detergents such as linear alkyl-benzene sulfonate (LAS) were often found in Hpo-N [10,19]; Hpo-A has also been considered as a humic-like substance [14,19].

Judging from the polydispersity of each DOM fraction as well as the above references, Hpo-B and Hpi (monodispersed fraction) probably consist of relatively homogenous compounds such as aromatic amines and amino acids, respectively; whereas, Hpo-A (polydispersed fraction) consists of relatively heterogeneous compounds such as humic-like substances. Considered the weight-average molecular weight (M_w) is approximately twice the number-average molecular weight (M_n) value for a step-polymerization reaction product, it is expected that the Hpo-A of L-1, L-2, L-5 and L-13 are step-polymerization reaction product [1]; Hpo-A can be expected to be polymerized with ease compared to the other fractions.

4.3. Fluorescent properties of DOM fractions

DOM reveals fluorescent properties under visible and UV light due to either the presence of an aromatic nucleus substituted by at least one electron-donating group, or to a conjugated unsaturated system capable of a high degree of resonance [24]. As shown in Fig. 5, most of the DOM fraction in each sample showed similar peaks, but with different intensities, which implicates the existence of common fluorophores in different proportions in the DOM fraction of each sample [12].

In the LM1 samples, most of Hpo-B and Hpi showed high intensities at a relative longer wavelength (around 350 nm), and in contrast to Hpo-B and Hpi, Hpo-A of LM1 showed high intensity at a relatively shorter wavelength (around 310 nm). This shows that Hpo-A revealed a small degree of aromatic polycondensation and a small level of conjugated chromophores compared to both Hpo-B and Hpi. Also, the lower intensity at around 310 nm for Hpo-B and Hpi may reflect a relative smaller presence of electron-donating substituents such as hydroxyl and methoxy groups within this wavelength region compared to Hpo-A [23].

As shown in Fig. 6, most of the DOM fractions showed maximum intensities at around 278–294/298–314 or 320–336/340–356 nm (excitation/emission). According to [4,13,31], it would be expected that tyrosine-like and tryptophan-like fluorophores account for a large portion of the fluorophores in each DOM fraction. Especially, Hpo-A showed maximum intensity within the tyrosine-like fluorophore region except for L-2 and L-8, which contain abundant amounts of non-combustible wastes, and the closed landfill site (L-10). The DOM fractions that showed maximum intensities within the tryptophan-like fluorophore region were mainly Hpi and Hpo-B.

The fact that all three DOM fractions of L-2 and L-8 which abundantly contained non-combustible wastes showed a dominant peak at around 356 nm compared to another peak at around 300 nm implies that the structures of the fluorophores for L-2 and

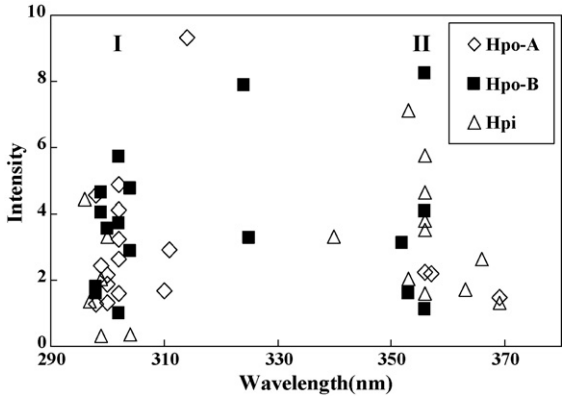

Fig. 6. Emission wavelength of maximum intensities of DOM fractions (I: tyrosine-like, II: tryptophan-like).

L-8 are more aromatic condensed and conjugated compared to the other landfill sites [23].

Moreover, laboratory experiments have demonstrated that authentic-free amino acids and protein added to seawater were incorporated into a refractory DOM, and subsequently protected against microbial degradation [31]. Hubberten et al. [9] reported that amino acids in hydrophobic (humic) DOM were resistant to bacterial utilization. From the above references, the aromatic amino acid-like fluorophores in the DOM fractions of landfill leachate may retard the biodegradation of DOM.

4.4. Interaction of DOM fractions with the pollutants

As with the Cu(II) titration results shown in Table 4, the maximum quenched wavelengths of most samples were around 300 nm or 350 nm, which may reflect the aromatic amino acids (tyrosine, tryptophan) like fluorophores play an important role in the complexation with Cu^{2+}.

The original Stern–Volmer plots of Hpo-B and Hpi generally deviated from linearity compared to that of Hpo-A, as shown in Fig. 7. According to the deviation from linearity and the downward curvature of the original Stern–Volmer plots for Hpo-B and Hpi, it would be expected that they contain many inaccessible fluorophores compared to Hpo-A [17]. Considered the tryptophan in proteins generally show inaccessible fluorophores in the process of collisional quenching with polar or charged quencher [17], the poor linearity and higher I_{res} of Hpo-B and Hpi were probably due to typtophan-like fluorophores.

As shown by the log K value in the Cu(II) titration results obtained using the modified Stern–Volmer equation, the general trend (log K for Hpo-A < log K for Hpo-B and Hpi) was found in all but a few samples. This means that the reactivities of accessible binding sites of Hpo-B and Hpi with Cu^{2+} are greater than those of Hpo-A. However, the log K value obtained from the original Stern–Volmer equation indicates the overall reactivity of Hpo-A with Cu^{2+} would be greater than those of Hpo-B and Hpi with the exception of a few samples (LM1, L-13). In addition, it could be judged from the maximum quenching wavelength (emission) that the fluorophores bound with Cu^{2+} in the DOM fractions at the final disposal sites containing abundant amounts of non-combustible wastes, and those with a long operating period are more aromatic condensed and conjugated.

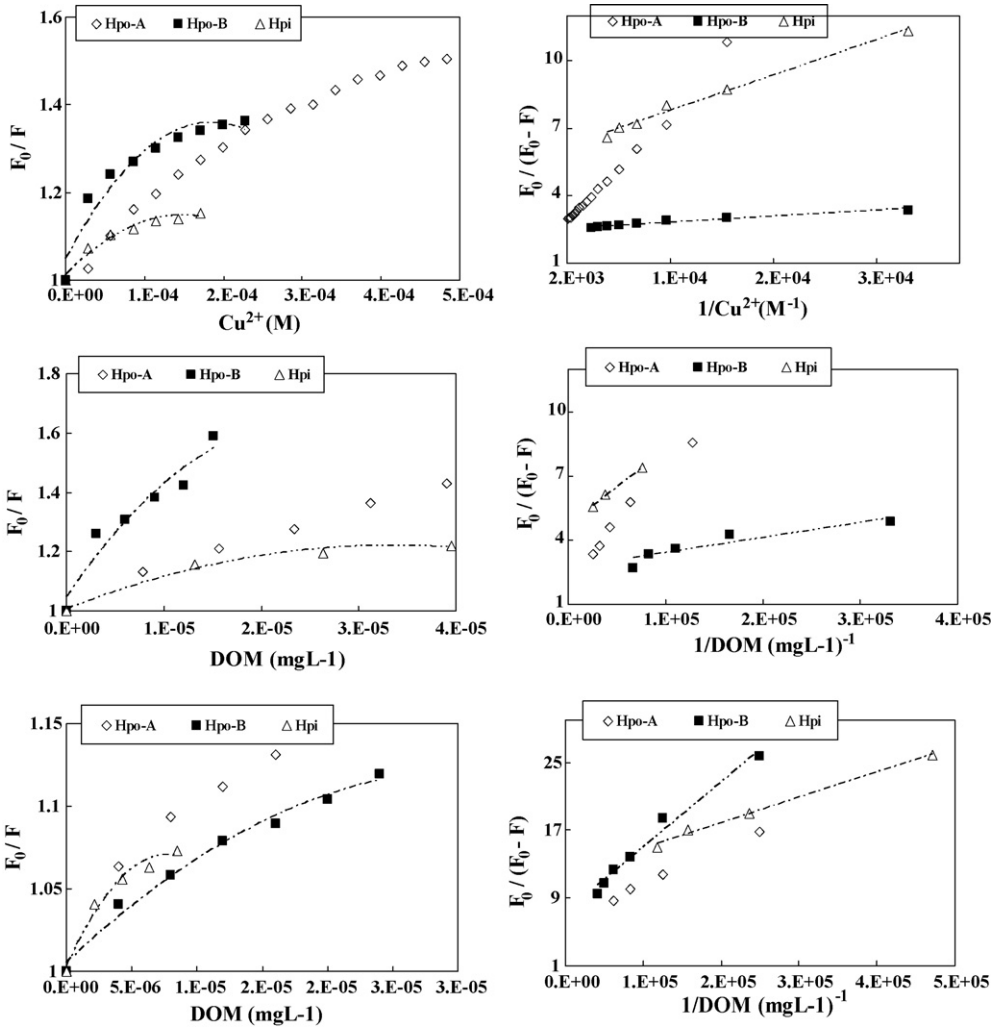

Fig. 7. The examples of titration results for Cu^{2+} (top, LM2), pyrene (middle, L-6) and phenanthrene (bottom, L-9) (left: original Stern–Volmer plots, right: modified Stern–Volmer plots).

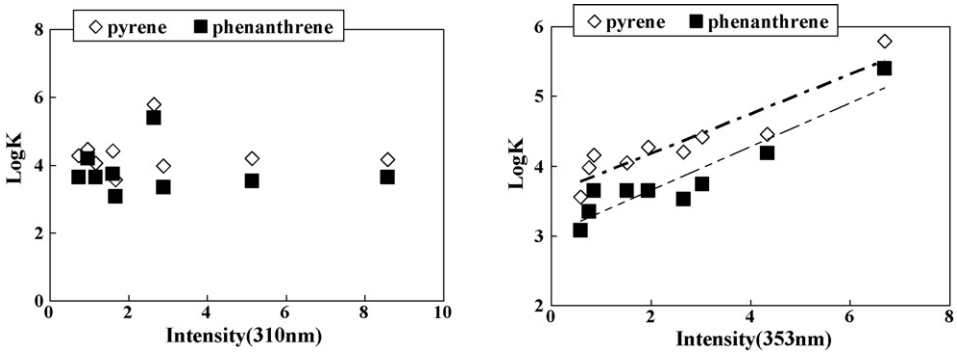

Fig. 8. The correlation between fluorescence intensity (at 310 and 353 nm) and log *K*.

As shown in the pyrene and phenanthrene titration results, the reason pyrene showed higher log *K* and lower I_{res} values than phenanthrene for each DOM fraction may have been due to two facts: (a) pyrene has one more aromatic ring compared to phenanthrene and (b) the aromatic ring affects the complexation with DOM. Moreover, the correlation between the log *K* value and the intensity of LM1 samples at 310 nm and 353 nm as shown in Fig. 8 was investigated to find the effect of fluorescence intensity and wavelength on the log *K* value. The reason LM1 samples were chosen is that they used the same operating conditions and commonly had simple peaks at around 310 nm and 353 nm. As shown in Fig. 8, the linear correlation between the fluorescence intensity and log *K* value at 310 nm was poor; however, the correlation at 353 nm showed good linearity (r_{pyrene}: 0.9259, $r_{phenanthrene}$: 0.9351). This indicates that log *K* values increase with increasing contents of aromatic condensed fluorophores substituted with electron-donating groups. For the landfill sites, a linear correlation between the fluorescence intensity (at relative longer wavelength region) and log *K* value was difficult to deduce. This appears to be due to variety of factors (e.g. molecular size and viscosity etc.) that can affect complexation.

Aromatic and aliphatic amines are efficient quenchers of most unsubstituted aromatic hydrocarbon [17]. From the results of this study, it is highly probable that aromatic amino acid-like fluorophores in the DOM fractions play an important role in complexation with PAHs.

4.5. Properties of DOM extracted from incineration residues

Although most combustible fractions of combustible wastes are turned into inorganic matter by the incineration process, a small amount of organic matter, i.e. loss on ignition (LOI), would remain in the incineration residues. The LOI in incineration residues contains aromatic substances including PAHs and other organic pollutants such as dioxins etc. generated in the incineration process as well as a small amount of not-yet combusted organic matter. In the early period of a landfills' use, the concentration of dissolved matter would be increased by the solubilization of readily degradable matters when organic matters in the landfill are decomposed by microorganisms. At this time, the dissolved matter is in a simply dissolved solid state corresponding to the Hpi fraction in this study.

The fact that LM2, L-2, L-8 and L-12 containing abundant amounts of incineration residues showed a lower proportion of Hpi compared to the other sites indicates that the most of the solubilizable fractions are removed by the incineration process.

5. Conclusion

For leachates discharged from final disposal sites containing MSWIRs, DOM fractionation using DAX-8 resin, GPC for molecular weight analysis, FTIR for functional group analysis and fluorescence analysis for fluorescent properties, as well as assessment of the binding sites of DOM fractions were carried out in this study.

Hpo-N generally increased with increasing operating period. However, this trend was not due to an increase in the concentration but because of an increase in the relative proportion from the decrease in the concentration of other DOM fractions. Landfill sites which contain abundant amounts of non-combustible wastes (i.e. MSWIRs) showed a higher proportion for Hpo-B and Hpo-N compared to Hpi and Hpo-A.

From the results of interaction of DOM and the pollutants, it was observed that aromatic amino acid-like fluorophores were main fluorophores in each DOM fraction and these fluorophores could be an important constituent affecting complexation with the pollutants. In the case of PAHs titration, the log *K* values increase with increasing contents of aromatic condensed fluorophores substituted with electron-donating groups. However, any trend of log *K* from the landfill sites was not found. Thus, it was very difficult to characterize the leachability of pollutants by the distribution trend of DOM fraction.

Considering the low DOM content, including suspended solids which play a significant role in the transportation of pollutants in the leachate discharged from landfill sites that contained abundant amounts of incineration residues, the leachabilities of pollutants by DOM would be weaker than from those containing abundant amounts of MSW.

Finally, considering all of results in this study, co-disposal namely, burying of MSWIRs (as a source of the pollutants) with abundant amounts of MSW (as a source of the transporter of pollutants such as DOM containing amino acid-like fluorophores)

could be a serious environmental concern in terms of leaching of pollutants. In brief, DOM (especially, humic-like substance) containing amino acid-like fluorophores would complex with the pollutants (e.g. heavy metals and POPs) in MSWIRs. DOM complexed with the pollutants may contaminate the groundwater when linear system has a leakage and also may flow into the environment when the leachate is not treated properly. Therefore, a method of landfill construction or operation to control the behaviors of pollutants is warranted.

Acknowledgement

This work was supported by grant No. R01-2005-000-10635-0 from the Basic Research Program of the Korea Science & Engineering Foundation.

References

[1] R.D. Archer, Inorganic and Organometallic Polymers, A John Willey & Sons, New York, 2001, pp. 99–107.
[2] D.J. Burdige, S.W. Kline, W. Chen, Fluorescent dissolved organic matter in marine sediment pore waters, Mar. Chem. 89 (2004) 289–311.
[3] J.B. Christensen, D.L. Jensen, Grøn Christian, Filip Zdenek, T.H. Christensen, Characterization of the dissolved organic carbon in landfill leachate-polluted groundwater, Water Res. 32 (1998) 125–135.
[4] P.G. Coble, Characterization of marine and terrestrial DOM in seawater using excitation–emission matrix spectroscopy, Mar. Chem. 51 (1996) 325–346.
[5] T.D. Gauthier, E.C. Shane, W.F. Guerin, W.R. Seitz, C.L. Grant, Fluorescence quenching method for determining equilibrium constants for polycyclic aromatic hydrocarbons binding to dissolved humic materials, Environ. Sci. Technol. 20 (1986) 1162–1166.
[6] J.S. Gaffney, N.A. Marley, S.B. Clark, Humic fulvic acids organic colloidal materials in the environment, in: J.S. Gaffney, N.A. Marley, S.B. Clark (Eds.), Humic and Fulvic Acids, American Chemical Society, 1996, pp. 1–16.
[7] E.H. Goslan, S. Voros, J. Banks, D. Wilson, P. Hills, A.T. Champbell, S.A. Parsons, A model for predicting dissolved organic carbon distribution in a reservoir water using fluorescence spectroscopy, Water Res. 38 (2004) 783–791.
[8] D. Hernández, C. Plaza, N. Senesi, A. Polo, Detection of copper(II) and zinc(II) binding to humic acids from pig slurry and amended soils by fluorescence spectroscopy, Environ. Pollut. 143 (2006) 212–220.
[9] U. Hubberten, R.J. Lara, G. Kattner, Amino acid composition of seawater and dissolved humic substances in the Greenland Sea, Mar. Chem. 45 (1994) 121–128.
[10] A. Imai, T. Fukushima, K. Matsushige, Y.H. Kim, K.S. Choi, Characterization of dissolved organic matter in effluents from wastewater treatment plants, Water Res. 36 (2002) 859–870.
[11] M.N. Jones, N.D. Bryan, Colloidal properties of humic substances, Adv. Colloid Interface Sci. 78 (1998) 1–48.
[12] Joaquim C.G. Esteves da Silva, Adélio A.S.C. Machado, César J.S. Oliveira, Marta S.S.D.S. Pinto, Fluorescence quenching of anthropogenic fulvic acids by Cu(II), Fe(III) and UO_2^{2+}, Talanta 45 (1998) 1155–1165.
[13] Juhani Peuravuori, Riitta Koivikko, Kalevi Pihlaja, Characterization, differentiation and classification of aquatic humic matter separated with different sorbents: synchronous scanning fluorescence spectroscopy, Water Res. 36 (2002) 4552–4562.
[14] K. Kalbitz, S. Geyer, W. Geyer, A comparative characterization of dissolved organic matter by means of original aqueous samples and isolated humic substances, Chemosphere 40 (2000) 1305–1312.
[15] Y.J. Kim, D.H. Lee, M. Osako, Effect of dissolved humic matters on the leachability of PCDD/F from fly ash—laboratory experiment using Aldrich humic acid, Chemosphere 47 (2002) 599–605.
[16] Y.J. Kim, M. Osako, Investigation on the humification of municipal solid waste incineration residue and its effect on the leaching behavior of dioxins, Waste Manage. 24 (2004) 815–823.
[17] J.R. Lakowicz, Principles of Fluorescence Spectroscopy, second ed., Kluwer Academic/Plenum Publishers, New York, 1999.
[18] J.A. Leenheer, R.L. Wershaw, G.K. Brown, M.M. Reddy, Characterization and diagenesis of strong-acid carboxyl groups in humic substances, Appl. Geochem. 18 (2003) 471–482.
[19] J.A. Leenheer, Comprehensive approach to preparative isolation and fractionation of dissolved organic carbon from natural waters and wastewaters, Environ. Sci. Technol. 15 (1981) 578–587.
[20] N.A. Marley, J.S. Gaffney, K.A. Orlandini, Characterization of aquatic humic and fulvic materials by cylindrical internal reflectance infrared spectroscopy, in: J.S. Gaffney, N.A. Marley, S.B. Clark (Eds.), Humic and Fulvic Acids, American Chemical Society, 1996, pp. 96–107.
[21] D.K. Ryan, J.H. Weber, Copper(II) complexing capacities of natural waters by fluorescence quenching, Environ. Sci. Technol. 16 (1982) 866–872.
[22] K.-W. Schramm, M. Merk, B. Henkelmann, A. Kettrup, Leaching of PCDD/F from fly ash and soil with fire-extinguishing water, Chemosphere 30 (1995) 2249–2257.
[23] N. Senesi, T.M. Miano, M.R. Provenzano, G. Brunetti, Characterization, differentiation, and classification of humic substances by fluorescence spectroscopy, Soil Sci. 152 (1991) 259–271.
[24] B.K. Seal, K.B. Roy, S.K. Mukherjee, Fluorescence emission spectra and structure of humic and fulvic acids, J. Indian Chem. Soc. 41 (1964) 212.
[25] E.M. Thurman, R.L. Malcolm, Preparative isolation of aquatic humic substances, Environ. Sci. Technol. 15 (1981) 463–466.
[26] E. Tipping, Modelling ion binding by humic acids, Colloids Surf. A: Physicochem. Eng. Aspects 73 (1993) 117–131.
[27] E. Tipping, Modelling Al competition for heavy metal binding by dissolved organic matter in soil and surface waters of acid and neutral pH, Geoderma 127 (2005) 293–304.
[28] H.A. Van der Sloot, J.J. Dijkstra, Development of horizontally standardized leaching tests: a material based or release based approach? Identical Leaching Mechanism for Different Materials, ECN-C-04-060, June 2004.
[29] S.-M. Jeong, M. Osako, Y.-J. Kim, Utilizing a database to interpret leaching characteristics of lead from bottom ashes of municipal solid waste incinerators, Waste Manage. 25 (2005) 694–701.
[30] J. Wu, L.J. West, D.I. Stewart, Effect of humic substances on Cu(II) solubility in kaolin-sand soil, J. Hazard. Mater. B94 (2002) 223–238.
[31] Y. Yamashita, E. Tanoue, Chemical characterization of protein-like fluorophores in DOM in relation to aromatic amino acids, Mar. Chem. 82 (2003) 255–271.